Soft Matter

Accepted Manuscript

ROYAL SOCIETY OF CHEMISTRY

www.rsc.org/softmatter

Dynamics and Yielding of Binary Self-Suspended Nanoparticle Fluids

Akanksha Agrawal[1], Hsiu-Yu Yu[2], Samanvaya Srivastava[1], Snehashis Choudhury[1], Suresh Narayanan[3], Lynden A. Archer*[,1]

[1]*School of Chemical and Biomolecular Engineering, Cornell University, Ithaca, NY 14853, USA*

[2]*Department of Chemical and Biomolecular Engineering, University of Pennsylvania, Philadelphia, PA 19104, USA*

[3]*Advanced Photon Source, Argonne National Laboratory, Argonne, IL 60439, USA*

Abstract

Yielding and flow transitions in bi-disperse suspensions of particles are studied using a model system comprised of self-suspended spherical nanoparticles. An important feature of the materials is that the nanoparticles are uniformly dispersed in the absence of a solvent. Addition of larger particles to a suspension of smaller ones is found to soften the suspensions, and in the limit of large size disparities, completely fluidize the material. We show that these behaviors coincide with a speeding-up of de-correlation dynamics of all particles in the suspensions and are accompanied by reduction in the energy dissipated at the yielding transition. We discuss our findings in terms of ligand-mediated jamming and un-jamming of hairy particle suspensions.

Introduction

Suspensions of small particles are of increasing scientific interest as model systems for studying structure, dynamics, and phase transitions in atomic and molecular liquids.[1–6] On imposition of pressure, thermal, or concentration fields, suspensions of micron-sized particles exhibit features such as disordered structure,[7] jamming/glass transitions,[5,8–10] aging,[11,12] and solid/liquid phase transitions[13–15] traditionally found in molecular liquids.

Recently, soft colloids have emerged as attractive model systems for molecular fluids because they are able to capture both excluded volume and more complex interactions in such fluids. Among the most unexpected observations are recent findings of reduced inter-particle correlation, disordering, and faster relaxation as the particle concentration approaches the jamming transition.[16–19] These observations have been shown to have some similarities to the cascade of anomalies reported in complex liquids such as water.[20–22] The ability of a suspension of soft colloids to reproduce these physics has been attributed to polydispersity in particle size brought about by soft particle-particle contacts and deformation. Here we wish to study these behaviors in model bi-disperse suspensions of soft particles.

The phase behavior, dynamics and structure of binary suspensions of soft colloids are also important for practical reasons. Recently, Schaefer et al. reported that a jammed suspension of hairy nanoparticles grafted with ion-conducting polymers and salts, spontaneously forms structured electrolytes with attractive conductivity values.[23] By internalizing chemistry introduced on the surface of nanoparticles into the nanopores, these electrolytes provide powerful tools for ion rectification and for stabilizing electrodeposition of metals.[24] A binary dispersion of such particles, in which the smaller diameter component loosens packing constraints on the larger ones, provides additional degrees of freedom for manipulating nanopore geometry, surface chemistry, and for enhancing charge transport.[25] For a binary hard-sphere particle blend with size ratio r=D_s/D_L, where D_s and D_L are the diameter of the small and big spheres respectively, density functional theory[26–28] and simulations by recent (mode-coupling theory) MCT calculations[29,30] show that the structure depends on the total volume fraction of the

particles and r. In particular for r <0.2, changing the fraction of small particles and the overall particle volume fraction leads to a series of transitions between glassy phases: From (I) a partially frozen repulsive single glass; to (II) a depletion-induced attractive glass; to (III) a fully frozen double glass; and finally to (IV) a small-particle driven "torroncino" phase. The theory also predicts that depletion-induced bonding for large size disparities of r <0.2 will lead to loose aggregates of the larger particles. Recent experiments[31,32] using binary hard spheres with r <0.2 show that these depletion forces exist and that the resultant binary particle systems exhibit dynamic similarities to attractive glasses.[33–35] Experiments on bi-disperse mixture of star polymers[36,37] in solution also report a transition from a so-called single glass to a double glass by varying the size ratio at a fixed star volume fraction.

In this article, we report on rheology and dynamical transitions in a bi-disperse blend of hairy, self-suspended spheres. Created by densely grafting short polymer chains to the surface of silica nanoparticles of different sizes, these suspensions are characterized by a dilute, uniform distribution of mobile particles in the absence of solvent.[38,39] By keeping the chemistry and molecular weight of the grafted polymer fixed, we are able to eliminate complications from solvent-particle or solvent-polymer enthalpic interactions,[40,41] allowing the role played by entropic factors to be isolated and studied.

Experimental Methodology

1. Material and synthesis

Silica nanoparticles with diameters 10±2nm(Ludox SM-30, Sigma Aldrich), 25±3nm(Ludox TM-50, Sigma Aldrich), 50±5nm(Nanocomposix Inc), 80±4nm(Nanocomposix Inc), 200±8nm(Nanocomposix Inc), and 360±10nm(Stöber

synthesis[42]) were grafted by covalent attachment of polyethylene glycol(PEG, MW~5000 $gmol^{-1}$, Polymer Source) using a previously described synthesis procedure.[43] The polydispersities in the particle sizes is estimated from maximum entropy method using IRENA package[44], as shown in Figure S1 and the standard deviation for each particle size was obtained by fitting a Gaussian distribution. The grafting densities of the chains on the silica cores, computed from analysis of the residual inorganic content using thermal gravimetric analysis (TGA, TA instruments Q500) were found to be 1.4 chains/nm^2, 2.1 chains/nm^2, 1.8 chains/nm^2, 1.2 chains/nm^2, 2.0 chains/nm^2 and 1.2 chains/nm^2, respectively. The suspensions can be characterized using two parameters:(i) The particle size ratio, $r = D_s / D_L$, where D_S and D_L are, respectively, the diameter of the smaller and larger SiO_2 core particles; and (ii) The fraction, $x_L = \phi_L / (\phi_s + \phi_L)$, of the larger SiO_2 particles in the suspension. Here ϕ_L and ϕ_S are the respective volume fractions of large and smaller particles. Silica particles tethered with PEG are first dissolved in chloroform, which is a good solvent for silica and PEG. Particles of different sizes were mixed with 10nm size particles in different x_L fractions, while continuously stirring the solution. Chloroform was evaporated by keeping the sample vial on a hot plate and continuously stirring it to ensure uniform particle mixing. The sample was subsequently kept under vacuum for two days, to ensure complete solvent evaporation and to remove any residual strain in the system. For the systems studied here, D_S=10nm, while D_L is varied such that r=0.4, 0.2, 0.125, 0.05 and 0.027. The fraction of larger particles, x_L ranges from 0 to 1

with total core volume fraction, ϕ is around 0.12-0.15 for all the systems (Figure S2). The total core volume fraction can be given as- $\phi = \frac{(\frac{w_s}{\rho_s})}{(w_s(\frac{1}{\rho_s}-\frac{1}{\rho_p})+\frac{1}{\rho_p})}$.

Where, ρ_s and ρ_p are the densities of silica and PEG respectively and w_s is the weight fraction of silica as determined from TGA.

The dispersion state of the materials with different size ratios was observed using Transmission Electron Microscopy (TEM). The samples for TEM were prepared by solvent casting method. Dilute suspensions of the nanoparticles in chloroform were dropped on copper grids, which were subsequently annealed at 65°C for 24 hrs to ensure complete evaporation of chloroform and uniform particle dispersion.

2. Small Angle X-ray Scattering (SAXS) measurements

Small angle X-ray scattering (SAXS) measurements were performed on the binary systems with size ratio r=0.4 at Sector-12-ID-B of Advanced Photon Source(APS) at Argonne National Laboratory using a point collimated X-ray beam. All the samples were smeared on a thermal sample cell and the measurements were performed at 90°C, which is above the melting point of PEG. The measured scattering intensity $I(q)$ as a function of wave vector q, can be divided into contributions from the individual particles and from inter-particle correlations as $I\left(q,R_S,R_L,x_L,\phi_L\right)=P\left(q,R_S,R_L,x_L\right)S\left(q,R_S,R_L,x_L,\phi_L\right)$, with P and S denoting the form and the structure factors, respectively. In the limit of infinite dilution, $S\left(q,R_S,R_L,\phi_S\to 0,\phi_L\to 0\right)\sim 1$, and the form factors can be conveniently

estimated from the scattering intensities. SAXS measurements on dilute aqueous binary suspensions(1% volume fraction) of charge stabilized silica nanoparticles at different x_L values were performed to obtain the form factor. The measured form factor $\overline{P}$ for each binary suspension diluted in water is in good agreement with expectations based upon the mole fraction-weighted form factors for the pure species (Figure S3).[45–47] Thus, S could be facilely obtained as $S = I / \overline{P}$, and provides a means for evaluating particle correlations in the binary systems.[45,48]

3. X-ray Photon Correlation Spectroscopy (XPCS) measurements

X-ray photon correlation spectroscopy (XPCS) measurements were performed on binary systems with r=0.4 in sector-8-ID-I of Advanced Photon Source at Argonne National Laboratory across a range of wave vector q at an x-ray photon energy of 7.35keV. All the samples were kept in vacuum and the measurements were carried out by precisely controlling the temperature at 90°C to eliminate any external fluctuations.[49] XPCS measures the intensity auto-correlation function, which is defined as:

$$g_2(q,t) = \frac{\langle I(q,t')I(q,t'+t)\rangle}{\langle I(q,t')\rangle^2} \qquad (1)$$

Here I$(q,$t'**)** is the intensity measured at wave vector q at time t'.[50–52] $g_2(q,t)$ is related to the normalized intermediate scattering function (ISF, f (q**,**t)) through the Siegert relation:

$$g_2(q,t) = 1 + b\left|f(q,t)\right|^2 \qquad (2)$$

Here b is the instrument optical contrast. Previous studies[49,50,53] have shown that the ISF and subsequently the $g_2(q,t)$ can be fitted using a stretched exponential form:

$$f(q,t) = \exp[-(t/\tau)^{\beta}] \qquad (3)$$

Where τ and β are the characteristic relaxation time and stretching exponent of the ISF.

3. Rheology measurements

Dynamic rheological properties were studied using frequency- and strain-dependent oscillatory shear measurements at 90°C. A MCR501 (Anton Paar) mechanical rheometer equipped with a 10mm diameter, 2° cone-and-plate fixtures was used for these experiments. Prior to data collection, all the suspensions were pre-sheared by applying a variable shear strain ranging from 0.1% to 100% at a frequency of 10rad/s. This was done until the data was reproducible and the measurements were taken immediately after pre-shearing. Variable amplitude oscillatory shear measurements were performed at a fixed angular frequency of ω=10 rad/s and frequency-dependent oscillatory measurements were performed at a fixed shear strain of γ = 0.5%, chosen to fall well within the linear viscoelastic regime for all the materials studied. The time sweep measurements to observe any aging in the system were also done at a strain of γ = 0.5% and an angular frequency of ω=10 rad/s, with the time of measurement as long as $6\text{x}10^4$ s.

Results and Discussion

Figure 1a)-d) reports typical transmission electron micrographs for bi-disperse hairy particle suspensions with different size ratios at $x_L = 0.2$. It is apparent from Figures 1a) and b) that for moderate size ratios of $r = 0.4$ and 0.2, both the small and big particles are well-dispersed. At the same time, Figures 1c) and 1d) indicate that on progressing towards lower size ratios, the bigger particles tend to form clusters, consistent with the

presence of depletion attraction between the larger particles induced by the smaller particles.[31]

The well-dispersed state of bi-disperse systems with $r = 0.4$ is further confirmed from SAXS experiments. It can be observed from Figure 1e) that the scattering intensities $I(q)$ are at most weakly dependent on the wave vector at low q values, and exhibit a q^{-4} scaling at high q values, both of which are characteristics of well-dispersed spherical nanoparticles.[54,55] Figure 2a) reports the static structure factor for a range of x_L values at fixed $\phi \sim 0.15$ for $r = 0.4$. The position of the first maximum in S is largely insensitive to x_L and remains fixed at $q \sim 0.46$ nm^{-1} for $x_L \leq 0.25$ and at $q \sim 0.22$nm^{-1}for $x_L \geq 0.4$, which correspond to the inter-particle correlation lengths for self-suspended suspensions of the pure small and big particles, respectively. Remarkably, these trends are mirrored in $S(q)$ computed for semi-dilute bi-disperse hard sphere suspensions using the Percus-Yevick approximation.[56] The location of the first peak of the calculated S is seen to transition from $q \sim 0.5$nm^{-1} to $q \sim 0.25$nm^{-1} on increasing x_L over the same range.

The latter results can be understood by resolving the HS structure factor into three components (Figure S4) —S_{11}, S_{12} and S_{22}, where the subscripts 1 and 2 denote small and large particles, respectively. At high volume fractions of the smaller particles, i.e. $x_L < 0.3$, S_{11} dominates, while S_{22} contributes the most to the overall S as the volume fraction of bigger particles approaches unity. It is also noted that the contribution from S_{12} is always dwarfed by S_{11} or S_{22} and the first maximum in S is therefore predominantly determined by either S_{11} or S_{22}. Therefore, the similarity between the variation of the first maximum in $S(q)$ for our self-suspended systems and hard spheres reflects the dominant structural contributions from the silica nanocores.

The space filling constraints imposed on the tethered ligands that suspend the particles has been noted previously to produce a more uniform particle dispersion than achieved with hard spheres, which manifest as unique features in the structure factor.[57,58] In particular, the strong chain mediated correlations among the core particles lead to higher primary peaks, while the space filling constraint suppresses concentration fluctuations and results in a more rapid decay and lower S values in the low q regime. These features are conveniently captured in the S value at q = 0.22nm^{-1}(Figure 2b)). For large particle dominated systems ($x_L \geq 0.7$), q = 0.22nm^{-1} corresponds to the position of the primary correlation peak in S, and the $S_{q\sim0.22nm}^{-1}$ values deviates positively from the corresponding hard sphere values, characterizing a stronger chain-mediated inter-particle correlation.

Meanwhile, for $x_L \leq 0.7$, $S_{q\sim0.22nm}^{-1}$corresponds to the low-q regime where $qR < 1.5$ with R being the average core radius, and the $S_{q\sim0.22nm}^{-1}$ values deviate negatively from the corresponding hard sphere values, denoting the suppression of system density fluctuations by the space-filling oligomers. Figure 2c illustrates this result more clearly by comparing $S(q\text{->}0)$ for the hairy particle blends with the calculated values for hard sphere suspensions. The $S(0)$ values for the experimental systems were obtained by fitting the measured $S(q)$ to a quadratic function and extrapolating to q=0. It is apparent that $S(0)$ for the self-suspended hairy nanoparticles is always lower than for the corresponding binary hard sphere suspensions, which means that the self-suspended particles indeed have a more uniform dispersion than a suspension of hard spheres due to the space-filling constraint on the tethered ligands. In either case, however, increasing polydispersity leads to larger concentration fluctuations and therefore higher $S(0)$ values. Thus, we conclude that the inherent physical characteristics of the individual particles

used for the experiments (a hard core and soft corona) are preserved in the structure of the bi-disperse suspensions. We may also conclude that the polymers tethered to the nanocores not only play a very significant role in dispersion of these particles, but because of the requirement that they fill the inter-particle space, may also contribute to unique system dynamics.

To further examine the effect of polydispersity on particle-particle correlations, we probed the dynamics of fluctuations in particle correlations using X-ray photon correlation spectroscopy (XPCS). Figure S5a) shows that the loss and storage moduli show a very weak dependence on time, implying that the materials used for the study show negligible aging.[59] This is also confirmed by negligible variation in $g_2(q,t)$ over a time span of 3600s (Figure S5b)), which is higher than the relaxation time scales observed in XPCS measurements of our systems. Figure 3a) shows the evolution of the auto-correlation function, $g_2(q,t)$ for different binary particle mixtures. A terminal relaxation regime ($g_2(q,t) \sim 1$ at large time) is observed in every case, which is unusual for jammed colloidal suspensions comprising of soft spheres.[17] However, as reported earlier, the suspensions of densely-grafted hairy nanoparticles are able to reach an equilibrium state[39,60] and our observations therefore concurs with the absence of aging in these systems discussed above.

All particle blends also consistently exhibit a $\tau \sim q^{-1}$ relationship (Figure 3b) and c)), with $\beta \sim 1.5$ (Figure S6). This finding is in agreement with previous observations that the single-component self-suspended particles are jammed and exhibit slow, hyper-diffusive dynamics.[16,50,61] τ values for different systems were extracted at a fixed wave vector, $q \sim 0.22\text{nm}^{-1}$, which corresponds to the inter-particle distance for large particles, and are

reported in Figure 3d) as a function of x_L. It can be seen that the de-correlation time decreases with increasing x_L until $x_L \approx 0.7$ and then rises again. This means that addition of either smaller or larger particles to a system of pure larger or smaller particles, respectively, leads to faster dynamics. Since the particles are well-dispersed and un-aggregated, this speeding-up of dynamics cannot be a result of depletion induced interaction as reported previously.[32] The faster particle dynamics observed upon initial addition of either species is more likely the result of reduced correlations among particles. This increased entropy in bi-dispersed particle systems appears to be a consequence of the heterogeneity introduced due to polydispersity in size and variation in the oligomer volume carried by the smaller/bigger particles in the mixtures. Specifically, we propose that since the larger and smaller particles are defined by differences in curvature and the number of oligomers they carry per unit volume, addition of a different sized hairy particle to a pure self-suspended suspension of particles of another size increases heterogeneity and relaxes the space filling constraints on ligands tethered to their large/smaller cohorts. Since it is the ligand mediated interactions between the particles that lead to jamming at the low particle volume fractions studied here, the faster dynamics can be interpreted as a ligand-induced softening of the suspensions.

We expect these dynamical effects to have consequences on the rheological properties of the materials. Oscillatory shear rheology is an established method for studying the mechanical properties of suspensions and other soft glassy materials. Figure S7a) shows the frequency-dependent dynamic moduli for a bi-disperse system with r = 0.4. The observed response is typical of any soft glass, with $G' >> G''$ and a distinct minimum in G'', which is a reflection of structural relaxations inside the cage.[4,35] It is also noteworthy

that the minimum in G'', occurs at an angular frequency of ω=10rad/s for all the x_L values. Hence, the large amplitude oscillatory shear measurements for the systems were performed at this frequency. At larger strain amplitudes, the measurements can be used to obtain more detailed information about the strength and longevity of cage constraints. Figure 4a) reports a typical response to shear strain for the pure self-suspended suspension as well as for a typical bi-disperse material. It can be observed that the pure species show a single maximum in G'', which is associated with a single-step yielding transition in a soft glass[4,33,34,62–65] and has been attributed to strain-induced breakage of the "cage" which constraints the motion of particles in the material. In contrast, the bi-disperse suspensions show a characteristic two-step yielding transition, indicating that the cage landscape is more complex.

Similar two-step yielding has been observed for attractive glasses and gels[33,35] and it has been attributed to the breaking of inter-particle bonds followed by cage escape. A weak stress-strain response reminiscent of two-step yielding has also been reported for a binary mixture of hard spheres in a solvent,[66] but in that case the observations were limited to one x_L value. Figure 4b) reports the loss modulus normalized by its zero strain value, $G''/G''_{\gamma\to 0}$ as a function of shear strain. It is evident that a clear and distinct two-step yielding transition is seen over a wide range of x_L, which implies that there are two cage environments in the bi-disperse hairy particle mixtures over a wide composition range. We propose that the first, lower strain, yielding event reflects the release of cage constraints for smaller particles as it occurs at strains similar to those where the pure small-particle suspensions show a clear one-step yielding transition. The second yielding

event is attributed to release of constraints on bigger particles and thus occurs at a higher strain value.

From the loss modulus one can estimate the energy dissipated per unit volume, U_d, in each cage-breaking event, after removing the contribution from the background dissipation by subtracting dissipation measured in the low amplitude linear viscoelastic regime. Specifically, we de-convolute the two peaks in G'' using a lognormal fit, (shown by dotted lines in Figure 4b), which allows U_d to be estimated using the formula:[67]

$$U_d = \int \sigma(t)\dot{\gamma}(t)dt \sim \int \sigma d\gamma \sim \int G''(\gamma)\gamma d\gamma \,. \qquad (1)$$

Figure 4c) reports U_d as a function of x_L for $r = 0.4$. The closed symbols represent energy dissipated in breaking the first cage while the open symbols reflect the second cage breakage event. Since, the first peak in the normalized G''(Figure 4b) is attributed to relaxation of constraints for smaller, more tightly jammed particles, it is apparent that even a minute fraction of large particles relaxes cage constraints on smaller ones and markedly lowers the energy dissipated upon cage breakage. Similarly, introduction of smaller particles to pure larger particles leads to a reduction in dissipated energy associated with the breaking of the second cage, attributed to release of cage constraints on the bigger particles. Increasing the content of bigger particles added to the pure smaller-particle system eventually leads to an increase in U_d for both cages.

The observation of a minimum of U_d at $x_L \sim 0.5$ is consistent with the appearance of a minimum in τ observed in Figure 3d). We hypothesize that both observations reflect heterogeneity of corona interactions between larger and smaller particles. In our solvent-

free self-suspended systems, the oligomers have to uniformly fill the interstitial space. Even for equal molecular weight corona molecules, differences in grafting density and/or curvature of the particles to which the molecules are grafted will produce differences in the ease/difficulty with which the tethered fluid is able to fill the inter-particle space. These changes are anticipated to manifest as different degrees of chain stretching among chains tethered to pure smaller, pure larger, and bi-disperse mixtures of the particles. The heterogeneity in corona structure in the bi-disperse mixtures should therefore lead to an effective disordering of the tethered ligands and a softening of the cage constraints. A correlation between the faster particle de-correlation dynamics and the energy dissipated upon cage breakage is then unsurprising. Our observation that addition of larger particles to a bi-disperse blend can reduce the extent of jamming is, nevertheless, quite different from previous reports, where adding larger particles to a suspension of smaller ones is typically found to facilitate vitrification due to arrest of both the particles in their cages.[36]

We test our hypothesis by looking at the trends in rheological behavior for different size ratios. At r = 0.2 we see similar trends as observed above, as shown in Figure S7b) and S8. Figure 4d) shows the energy dissipated in breaking the cage for r = 0.2. We find again that addition of bigger particles leads to a dramatic decrease in the dissipated energy for the smaller ones. It is noteworthy that the dissipated energies for r = 0.2 are much lower than r = 0.4, as the bigger particles bring in more oligomer volume and thus leads to a stronger relaxation of the cage constraints on the smaller ones. On progressing towards lower size ratios, we find that the systems progressively move towards a liquid phase. As seen from Figure 5a at r = 0.125, addition of just a small fraction of larger particles leads to a transition to a liquid phase with $G''>G'$. Further addition of larger

particles leads to a transition back to a jammed soft glassy behavior. A similar progression to liquid phase is observed for r = 0.05 (Figure 5b)) and r = 0.027 (Figure 5c)).

An important parameter which can be used to quantify this behavior is the loss tangent, tan (δ) = G''/G'. Since it is the ratio of loss modulus to storage modulus, it is an indication of the extent of elasticity of the system and a loss tangent value greater than unity can be loosely used to identify a transition to liquid phase. Figure 6a) and b) report loss tangent values obtained in the linear viscoelastic regime at a fixed angular frequency, ω = 10rad/s. Consistent with our observations from XPCS experiments and dissipated energy calculations, we find that for larger size ratios, addition of bigger particles to a suspension of pure jammed smaller particles weakens the suspension and further introduction of bigger particles retrieves the jammed state. However, for smaller size ratios, we observe that addition of bigger particles leads to an increase in tan (δ) well beyond unity, indicating a transition to a liquid-like regime. Further addition of bigger particles results in a decrease in the loss tangent. Thus, in contrast to previous studies on binary hard spheres,[66,68] we find that the effect of jamming/un-jamming produced by addition of larger particles to smaller ones in a bi-disperse blend is more sustained and distinct, even at moderate x_L values. This result is believed to be a direct manifestation of the change in the space filling constraint for the tethered oligomeric fluid with the introduction smaller/bigger particles to a mono-disperse system. The loss tangent results are complemented by the trends observed in plateau modulus and complex viscosity as a function of x_L for various size ratios. Figures 6c) and 6d) show the plateau modulus normalized with energy density, which is given as $k_BT/\langle R^3 \rangle$, where k_B is the Boltzmann

constant, T is the temperature and $<R^3>$ is the average of the cube of particle radius[66]; and the rescaled complex viscosity at ω=1rad/s measured from frequency sweep measurements. We observe that for larger size ratios of r=0.4 and 0.2, addition of bigger particles leads to a weaker storage modulus, and a decrease in complex viscosity, replicating the results obtained from dissipated energy and loss tangent. While for smaller size ratios, addition of larger particles, decrease the plateau modulus to below unity which indicates that the energy due to thermal motion of the particles is much higher and hence implies a transition to liquid regime. Similar trends are observed in normalized complex viscosity, where addition of larger particles leads to a drastic decrease in the viscosity values, and further addition leads to a transition to jammed state.

An experimental state diagram (Figure 7) can be constructed based on the observations from the rheological responses in Figure 6. At larger particle size ratios, an increase in x_L first weakens a suspension of pure smaller particles and, at higher x_L, leads to a transition back to a jammed state. On progressing towards smaller size ratios, an increase in x_L leads to a transition from a soft glass to liquid and then back to a jammed glass. The state diagram observed here is much similar to that of the binary soft spheres[36,37] however the, the size ratios at which this transition from glass to a liquid regime is seen are much smaller, and the transition to the liquid regime occurs at increasingly smaller x_L values. This is a consequence of the increasingly high heterogeneity in oligomer volume that is introduced as the particle size increases, and hence the quantity of the bigger particles required to relax the smaller particles becomes lesser. Previous studies on binary hard spheres have shown that for r < 0.1, smaller particles produce depletion induced interactions between the bigger particles, which in turn enable access of the smaller

particles to a larger bulk volume, with the result that the system transitions to a liquid phase.[31] However, the absence of a solvent in our self-suspended materials means that the increased volume available to the smaller particles increases the extent to which tethered chains must stretch to fill the inter-particle space. The bigger particles bring more oligomeric fluid volume, and thus relax constraints on the smaller ones considerably, resulting in a transition to a liquid state. The re-entrant glassy state observed here is again a double glass with dominant large particles as evident from the two-step yielding observed for r = 0.125 and 0.05 for the x_L values in this regime. A unique aspect of these systems is that we are able to capture their state transitions for different size ratios at dilute concentrations of cores. This can be contrasted with previous studies on binary hard spheres, where experiments are typically carried out at volume fractions as high as 0.58. A practical consequence, wherein the binary hybrid nanoparticles have been used as highly conducting electrolytes, have recently been reported.[25]

5. Conclusion

In conclusion, we have studied the structure, dynamics, and rheology of bi-disperse suspensions of solvent-free polymer-functionalized, soft nanoparticles. We find that dispersity in particle size has significant and unexpected effects on both the dynamics and rheology of the suspensions. Specifically, for moderate particle size ratios, r = 0.4 and r = 0.2, adding bigger particles to a system of pure, jammed smaller particle first weakens the glass, beyond which further increase in the concentration of bigger particles leads to jamming of the material. In contrast, for extremely small size ratios, we find that even a small fraction of large particles can completely unjam a suspension of smaller ones.

These findings are confirmed by XPCS and rheology measurements, where addition of bigger particles speeds up de-correlation dynamics of the system. They are further supported by calculations of the energy dissipated at the jamming transition, where it is seen that the energy dissipated in releasing cage constraints on bigger and smaller particles is lower in bi-disperse blends than in nominally monodisperse soft particle suspensions. Significantly, all of these features are observed at an effective particle volume fraction of 0.12-0.15, which is much lower than the hard sphere glass transition volume fraction. This indicates that the tethered polymer chains play a major role in particle dispersion and their soft glassy behavior. We argue that interactions between these chains, dictated by the space filling constraint in a solvent-free self-suspended material, are responsible for the observed, large effects of particle size polydispersity on structure, dynamics, and rheology of bi-disperse suspensions of soft particles.

Acknowledgement

This work was supported by the National Science Foundation, Award No. DMR–1006323 and by Award No. KUS–C1–018–02, made by King Abdullah University of Science and Technology (KAUST). Use of the Advanced Photon Source, operated by Argonne National Laboratory, was supported by the U.S. DOE under Contract No. DE–AC02–06CH11357. We acknowledge Prof. D. L. Koch for helpful discussions.

References

1 P. N. Pusey and W. V. Megen, *Phys. Rev. Lett.*, 1987, **59**, 2083–2086.

2 P. N. Pusey and W. V. Megen, *Lett. to Nat.*, 1986, **320**, 340–342.

3 P. N. Pusey, W. C. K. Poon, S. M. Ilett and B. P, *J. Phys. Condens. Matter*, 1994, **6**, A29–A36.

4 T. G. Mason and D. A. Weitz, *Phys. Rev. Lett.*, 1995, **75**, 2770–2773.

5 V. Trappe, V. Prasad, L. Cipelletti, P. N. Segre and D. a Weitz, *Nature*, 2001, **411**, 772–5.

6 J. Mattsson, H. M. Wyss, A. Fernandez-Nieves, K. Miyazaki, Z. Hu, D. R. Reichman and D. a Weitz, *Nature*, 2009, **462**, 83–6.

7 C. S. O'Hern, L. E. Silbert and S. R. Nagel, *Phys. Rev. E*, 2003, **68**, 011306–1–19.

8 A. J. Liu and S. R. Nagel, *Nature*, 1998, **396**, 21–22.

9 B. P. Tighe, E. Woldhuis, J. J. C. Remmers, W. van Saarloos and M. van Hecke, *Phys. Rev. Lett.*, 2010, **105**, 088303–1–4.

10 E. Stiakakis, D. Vlassopoulos and J. Roovers, *Langmuir*, 2003, **19**, 6645–6649.

11 D. Bonn, S. Tanase, B. Abou, H. Tanaka and J. Meunier, *Phys. Rev. Lett.*, 2002, **89**, 015701–1–4.

12 B. Abou, D. Bonn and J. Meunier, *Phys. Rev. E*, 2001, **64**, 021510–1–6.

13 S. P. Meeker, W. C. K. Poon, J. Crain and E. M. Terentjev, *Phys. Rev. E*, 2000, **61**, 6083–6086.

14 T. Zykova-Timan, J. Horbach and K. Binder, *J. Chem. Phys.*, 2010, **133**, 014705–1–10.

15 P. Levitz, E. Lecolier, A. Mourchid, A. Delville and S. Lyonnard, *Europhys. Lett.*, 2000, **49**, 672–677.

16 S. Srivastava, L. A. Archer and S. Narayanan, *Phys. Rev. Lett.*, 2013, **110**, 148302–1–5.

17 Z. Zhang, N. Xu, D. T. N. Chen, P. Yunker, A. M. Alsayed, K. B. Aptowicz, P. Habdas, A. J. Liu, S. R. Nagel and A. G. Yodh, *Nature*, 2009, **459**, 230–3.

18 X. Cheng, *Soft Matter*, 2010, **6**, 2931–2934.

19 X. Cheng, *Phys. Rev. E*, 2010, **81**, 031301–1–12.

20 A. Scala, F. W. Starr, E. La Nave, F. Sciortino and H. E. Stanley, *Lett. to Nat.*, 2000, **406**, 166–169.

21 J. R. Errington and P. G. Debenedetti, *Lett. to Nat.*, 2001, **409**, 1–4.

22 F. Sciortino, A. Geiger and H. E. Stanley, *Lett. to Nat.*, 1991, **354**, 218–221.

23 J. L. Schaefer, S. S. Moganty, D. A. Yanga and L. A. Archer, *J. Mater. Chem.*, 2011, **21**, 10094–10102.

24 J. L. Nugent, S. S. Moganty and L. A. Archer, *Adv. Mater.*, 2010, **22**, 3677–80.

25 A. Agrawal, S. Choudhury and L. A. Archer, *RSC Adv.*, 2015, **5**, 20800–20809.

26 M. Dijkstra, R. van Roij and R. Evans, *Phys. Rev. E. Stat. Phys. Plasmas. Fluids. Relat. Interdiscip. Topics*, 1999, **59**, 5744–71.

27 M. Dijkstra, R. van Roij and R. Evans, *Phys. Rev. Lett.*, 1998, **81**, 2268–2271.

28 R. Roth and S. Dietrich, *Phys. Rev. E*, 2000, **62**, 6926–6936.

29 T. Voigtmann, *EPL (Europhysics Lett.*, 2011, **96**, 36006–p1–p6.

30 W. Götze and T. Voigtmann, *Phys. Rev. E*, 2003, **67**, 021502–1–14.

31 A. Imhof and J. K. G. Dhont, *Phys. Rev. Lett.*, 1995, **75**, 1662–1665.

32 M. Sikorski, A. R. Sandy and S. Narayanan, *Phys. Rev. Lett.*, 2011, **106**, 188301–1–4.

33 K. N. Pham, G. Petekidis, D. Vlassopoulos, S. U. Egelhaaf, W. C. K. Poon and P. N. Pusey, *J. Rheol. (N. Y. N. Y).*, 2008, **52**, 649–676.

34 K. N. Pham, G. Petekidis, D. Vlassopoulos, S. U. Egelhaaf, P. N. Pusey and W. C. K. Poon, *Europhys. Lett.*, 2006, **75**, 624–630.

35 N. Koumakis and G. Petekidis, *Soft Matter*, 2011, **7**, 2456–2470.

36 E. Zaccarelli, C. Mayer, A. Asteriadi, C. Likos, F. Sciortino, J. Roovers, H. Iatrou, N. Hadjichristidis, P. Tartaglia, H. Löwen and D. Vlassopoulos, *Phys. Rev. Lett.*, 2005, **95**, 268301–1–4.

37 C. Mayer, E. Zaccarelli, E. Stiakakis, C. N. Likos, F. Sciortino, a Munam, M. Gauthier, N. Hadjichristidis, H. Iatrou, P. Tartaglia, H. Löwen and D. Vlassopoulos, *Nat. Mater.*, 2008, **7**, 780–4.

38 R. Rodriguez, R. Herrera, L. A. Archer and E. P. Giannelis, *Adv. Mater.*, 2008, **20**, 4353–4358.

39 P. Agarwal, H. Qi and L. A. Archer, *Nano Lett.*, 2010, **10**, 111–5.

40 A. Tuteja, P. Duxbury and M. Mackay, *Phys. Rev. Lett.*, 2008, **100**, 077801–1–4.

41 M. E. Mackay, A. Tuteja, P. M. Duxbury, C. J. Hawker, B. Van Horn, Z. Guan, G. Chen and R. S. Krishnan, *Science*, 2006, **311**, 1740–3.

42 G. H. Bogush, M. A. Tracy and C. F. Zukoski, *J. Non. Cryst. Solids*, 1988, **104**, 95–106.

43 S. Choudhury, A. Agrawal, S. A. Kim and L. A. Archer, *Langmuir*, 2015, **31**, 3222–3231.

44 J. Ilavsky and P. R. Jemian, *J. Appl. Crystallogr.*, 2009, **42**, 347–353.

45 B. D. Aguanno and R. Klein, *J.Chem.Soc.Faraday Trans.*, 1991, **87**, 379–390.

46 C. De Kruif and A. Vrij, *Colloid Polym. Sci.*, 1988, **1076**, 1068–1076.

47 B. Weyerich, J. Brunner-Popela and O. Glatter, *J. Appl. Crystallogr.*, 1999, **32**, 197–209.

48 R. Krause, B. D. Aguanno, J. M. Mendez-Alcaraz, G. Nagele, R. Klein and R. Weber, *J. Phys. Condens. Matter*, 1991, **3**, 4459–4475.

49 S. Mazoyer, L. Cipelletti and L. Ramos, *Phys. Rev. Lett.*, 2006, **97**, 238301–1–4.

50 R. L. Leheny, *Curr. Opin. Colloid Interface Sci.*, 2012, **17**, 3–12.

51 D. Lumma, L. B. Lurio, M. a. Borthwick, P. Falus and S. G. J. Mochrie, *Phys. Rev. E*, 2000, **62**, 8258–8269.

52 H. Guo, G. Bourret, M. K. Corbierre, S. Rucareanu, R. B. Lennox, K. Laaziri, L. Piche, M. Sutton, J. L. Harden and R. L. Leheny, *Phys. Rev. Lett.*, 2009, **102**, 075702–1–4.

53 A. Madsen, R. L. Leheny, H. Guo, M. Sprung and O. Czakkel, *New J. Phys.*, 2010, **12**, 055001.

54 O. Glatter and O. Kratky, *Small Angle X-ray Scattering*, Academic Press, New York, United Sta., 1982.

55 S. Srivastava, P. Agarwal and L. A. Archer, *Langmuir*, 2012, **28**, 6276–81.

56 N. W. Ashcroft and D. C. Langreth, *Phys. Rev. Lett.*, 1967, **156**, 685–692.

57 H.-Y. Yu and D. L. Koch, *Langmuir*, 2010, **26**, 16801–11.

58 H.-Y. Yu, S. Srivastava, L. A. Archer and D. L. Koch, *Soft Matter*, 2014, **10**, 9120–35.

59 P. Agarwal and L. A. Archer, *Phys. Rev. E*, 2011, **83**, 041402–1–5.

60 S. Srivastava, J. H. Shin and L. A. Archer, *Soft Matter*, 2012, **8**, 4097–4108.

61 S. Narayanan, D. Lee, A. Hagman, X. Li and J. Wang, *Phys. Rev. Lett.*, 2007, **98**, 185506–1–4.

62 P. Sollich, F. Lequeux, P. Hébraud and M. Cates, *Phys. Rev. Lett.*, 1997, **78**, 2020–2023.

63 P. Agarwal, S. Srivastava and L. A. Archer, *Phys. Rev. Lett.*, 2011, **107**, 268302–1–5.

64 M. E. Helgeson, N. J. Wagner and D. Vlassopoulos, *J. Rheol. (N. Y. N. Y).*, 2007, **51**, 297–316.

65 N. Koumakis, A. Pamvouxoglou, A. S. Poulos and G. Petekidis, *Soft Matter*, 2012, **8**, 4271–4284.

66 T. Sentjabrskaja, E. Babaliari, J. Hendricks, M. Laurati, G. Petekidis and S. U. Egelhaaf, *Soft Matter*, 2013, **9**, 4524–4533.

67 S. N. Ganeriwala and C. A. Rotz, *Polym. Eng. Sci.*, 1987, **27**, 165–178.

68 T. Sentjabrskaja, M. Hermes, W. C. K. Poon, C. D. Estrada, R. Castaneda-Priego, S. U. Egelhaaf and M. Laurati, *Soft Matter*, 2014, **10**, 6546–6555.

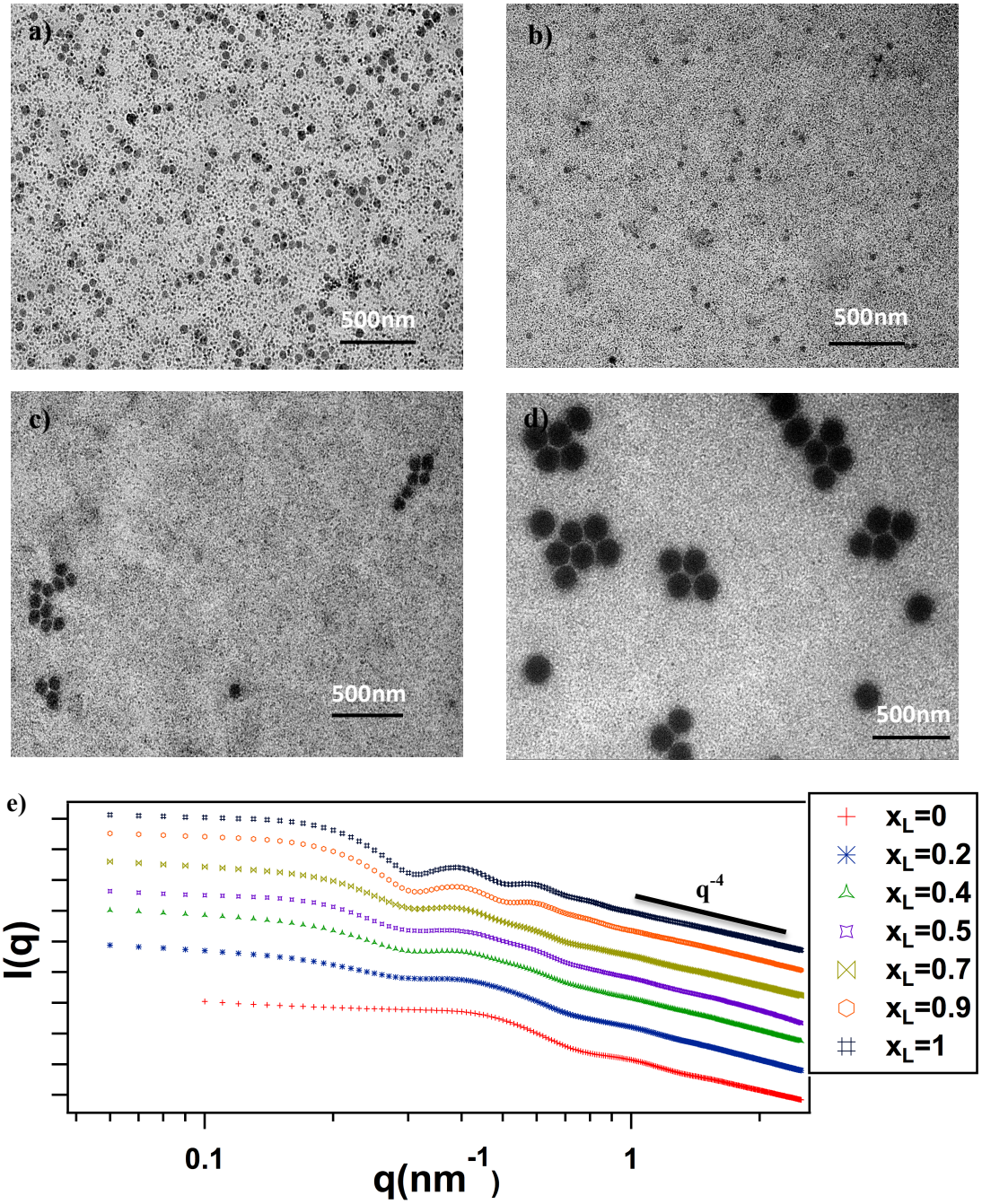

Figure1 Transmission electron micrograph for binary systems with **a)** $r = 0.4$ **b)** $r = 0.2$, **c)** $r = 0.125$ and **d)** $r = 0.05$ at x_L=0.2. **e)** Scaled intensities, $I(q)$ from SAXS experiments as a function of wave vectors on a log-log scale, from x_L=0 to 1, bottom to top for r=0.4.

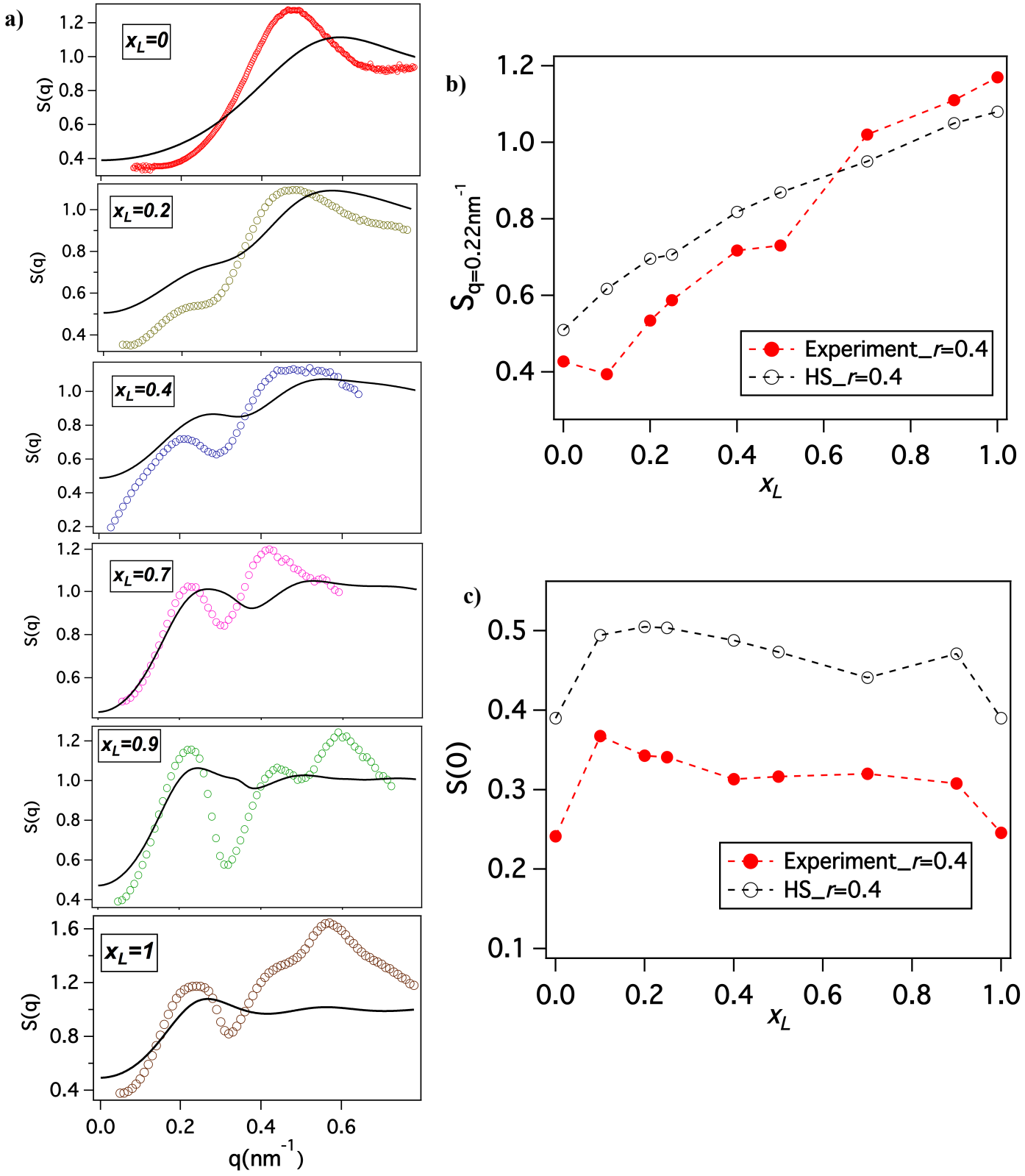

Figure 2a) Structure factor $S(q)$ vs q for systems with different x_L. The circles represent experimental result and lines are for HS calculations. Comparison of **b)** $S(q)$ at $q \sim 0.22nm^{-1}$ and **c)** $S(0)$ with HS calculations at different x_L.

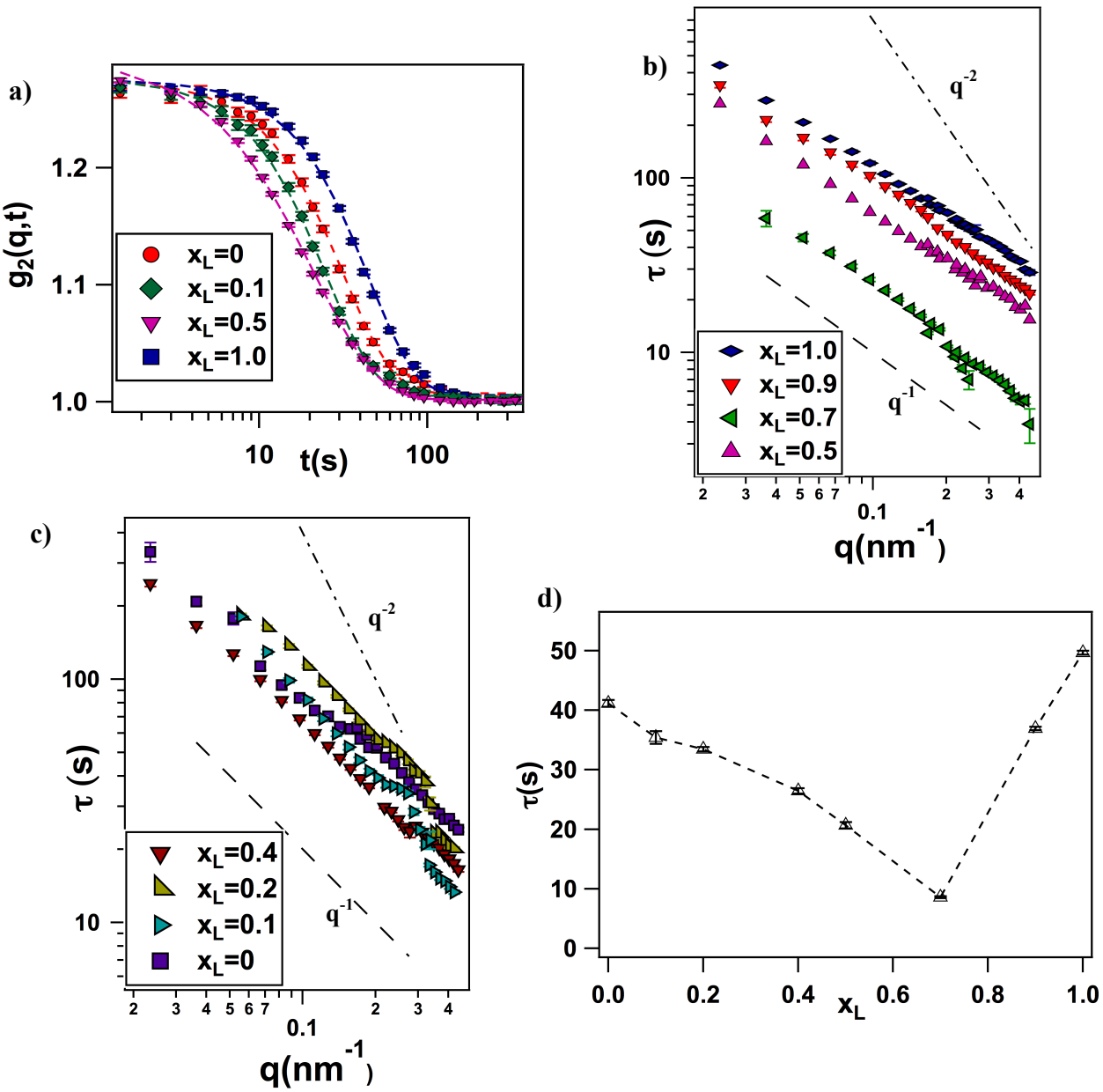

Figure 3a) Intensity auto-correlation function $g_2(q,t)$ at $q = 0.22\text{nm}^{-1}$ with stretched exponential fits. **b)** and **c)** Relaxation time τ as a function of wave vector q at different x_L. The dashed line denotes $\tau \propto 1/q$ scaling, and the dashed-dotted line denotes $\tau \propto 1/q^2$ scaling. **d)** Variation of τ with x_L at $q \sim 0.22\text{nm}^{-1}$. It can be seen that addition of either species first reduces the de-correlation time and then increases it.

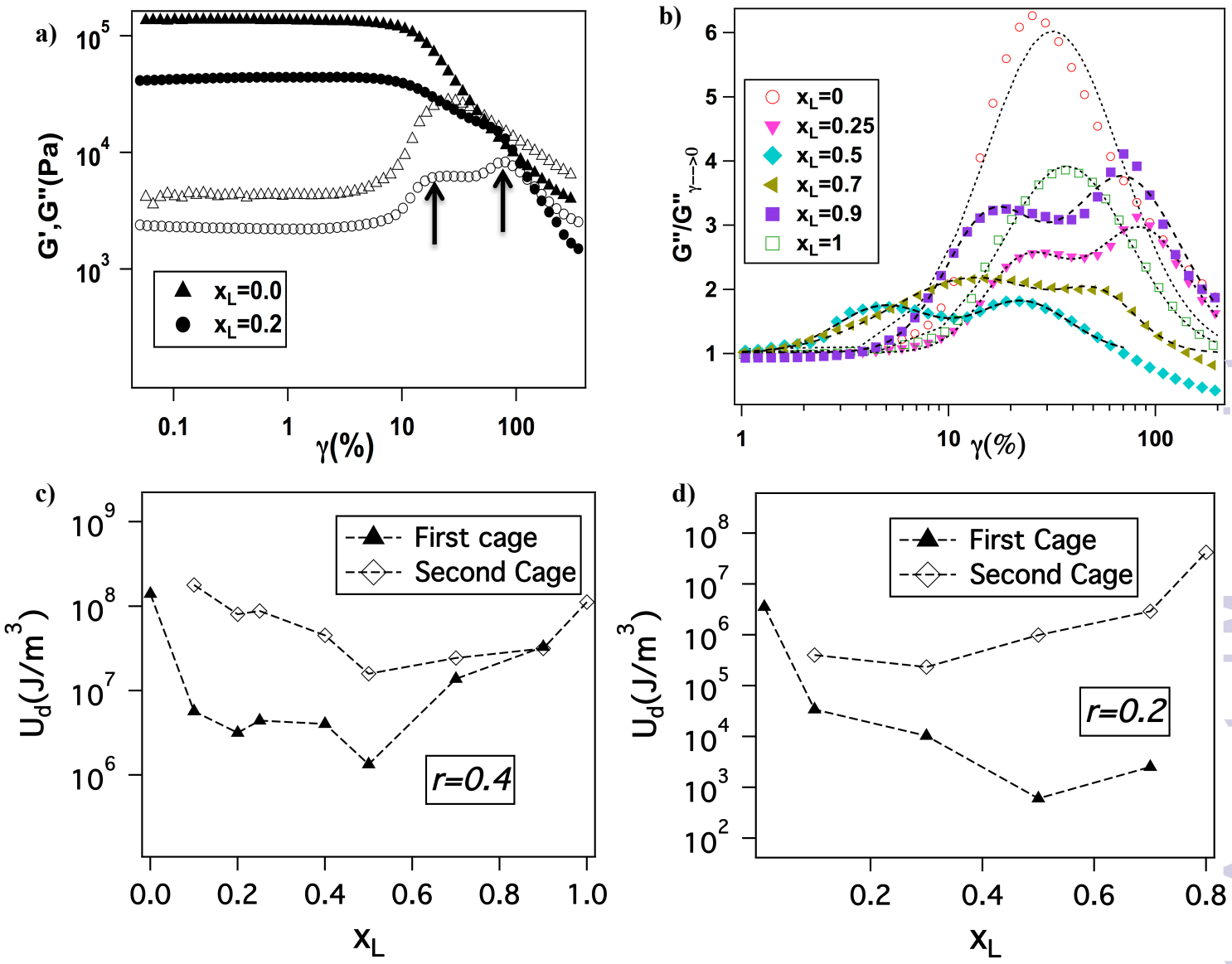

Figure 4a) Comparison of G′(closed symbols) and G″(open symbols) between a monodisperse ($x_L = 0$) and a binary system ($x_L = 0.2$) at $r = 0.4$. **b)** Normalized loss modulus, $G''/G''_{\gamma\to 0}$ at ω=10rad/s with lognormal fits (dotted lines) at $r = 0.4$. Energy dissipated in breaking the cage, U_d calculated from the normalized loss modulus for **c)** $r = 0.4$ and **d)** $r = 0.2$. The first cage corresponds to the constraints on the smaller particles while the second cage corresponds to the constraints set on larger particles.

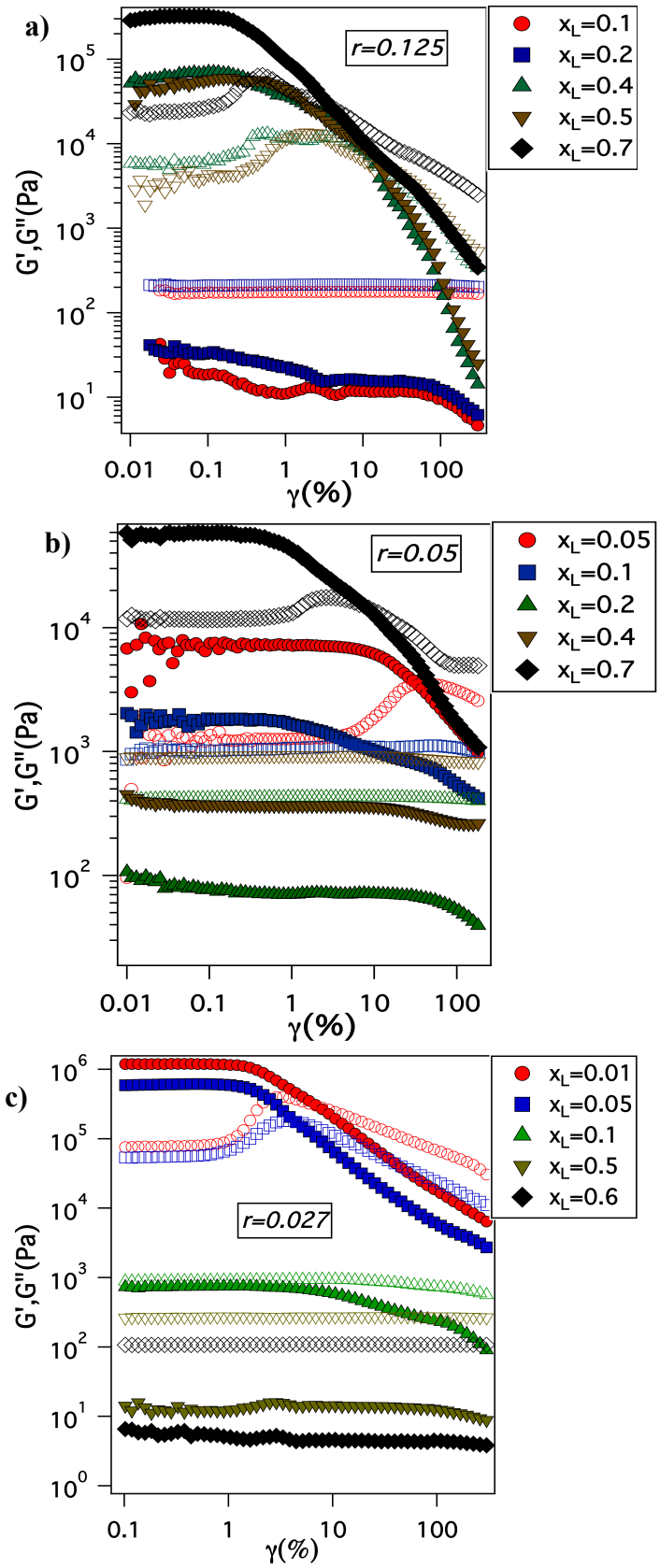

Figure 5 Amplitude sweep measurements of storage modulus, G'(closed symbols) and loss modulus, G''(open symbols) at ω =10rad/s for size ratios **a)** $r = 0.125$ **b)** $r = 0.05$ and **c)** $r = 0.027$. At $r = 0.125$ and $r = 0.05$, addition of bigger particles first leads to melting of glass, after which further increase in

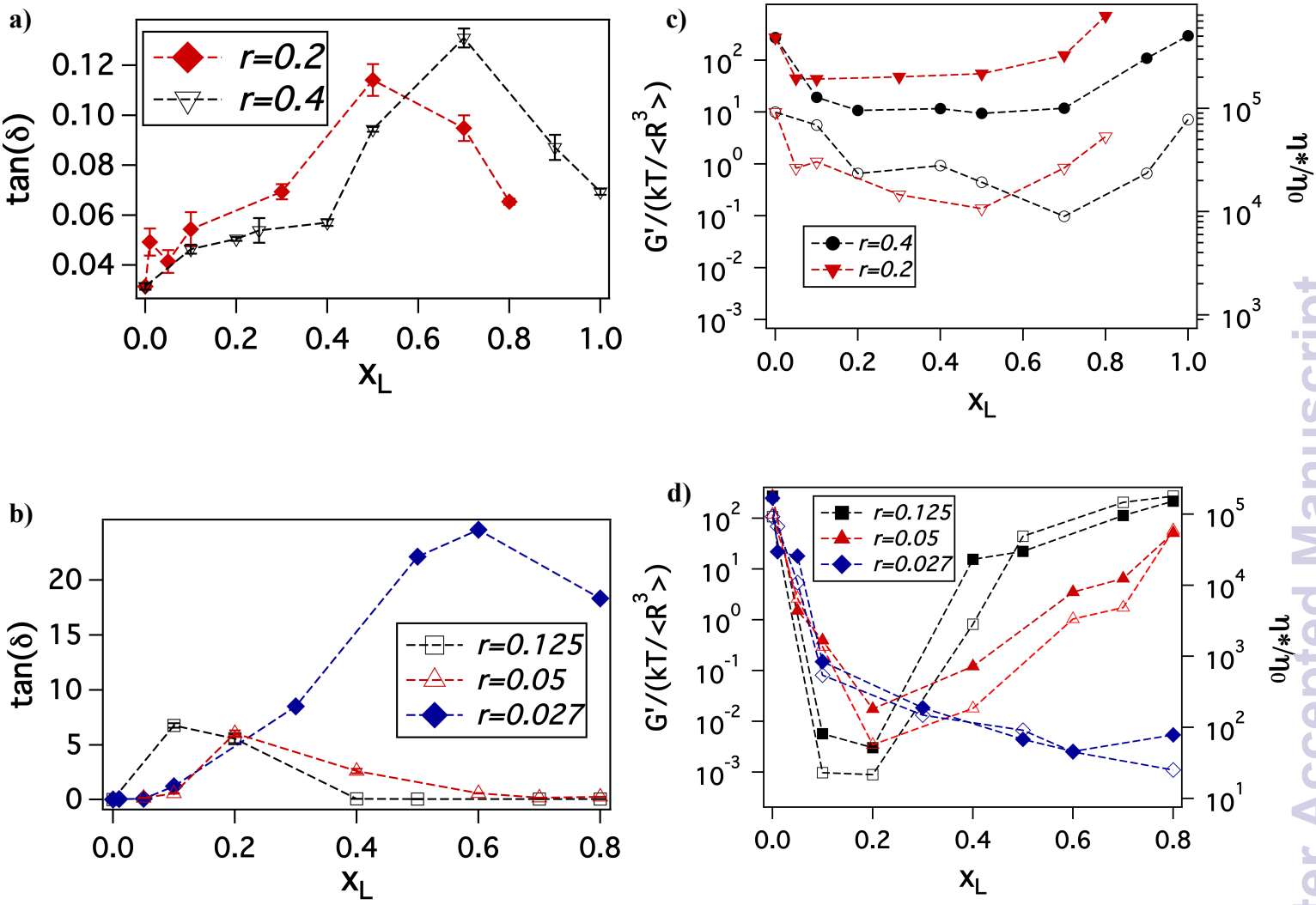

Figure 6 Comparison of loss tangent, tan (δ) at zero strain with increase in x_L at different size ratios **a)** r = 0.2 and r = 0.4, and **b)** r = 0.125, r = 0.05 and r = 0.027. Addition of bigger particles first leads to an increase in tan (δ), indicating particle unjamming and then a decrease in loss tangent. While for smaller size ratios of r = 0.125, r = 0.05 and r = 0.027, the loss tangent is greater than unity, indicating transition to liquid state. Plateau modulus normalized with energy density (closed symbols) and normalized complex viscosity(open symbol) measured at ω=1rad/s for **c)** r = 0.2 and r = 0.4, and **d)** r = 0.125, r = 0.05 and r = 0.027. η_0 corresponds to the complex viscosity to PEG(MW~5000g/mol) melt. The trends in normalized plateau modulus and complex viscosity confirm to the trends seen in loss tangent.

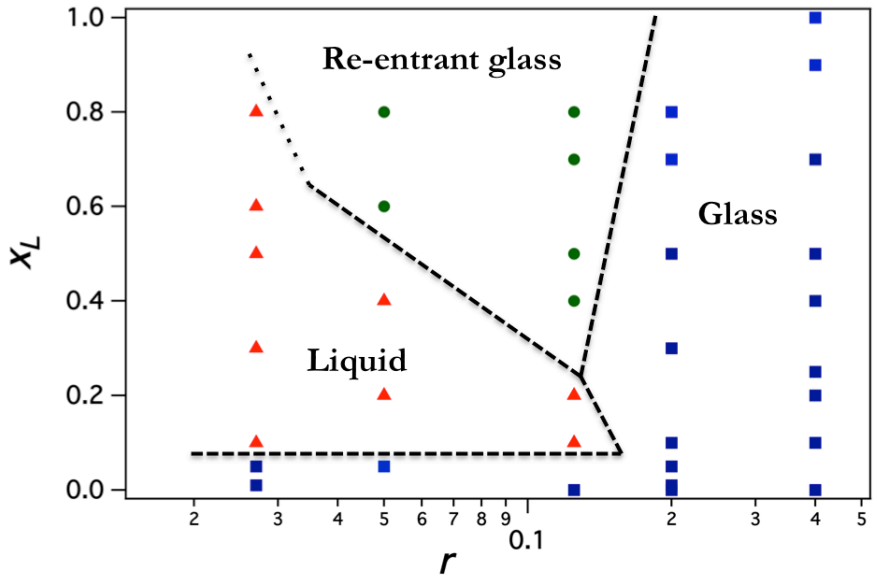

Figure 7 Experimental state diagram for x_L vs. size ratio, r. For smaller size ratios, increase in x_L leads to a weakening of glass, while for larger size ratios increase in x_L results in a transition from a soft glass to liquid and then again to an arrested glass.